International Journal of Recent Technology and Engineering (IJRTE)
ISSN: 2277-3878 (Online), 4 Issue-6, January 2016

Influence of Ball Material on Deformation in Non-Conforming Contact Ball Elements

Suresha Gowda M. V, Vidyasagar H. N, Ranganatha S

Abstract-The life of machine element is important in industry so that the equipment is more reliable and economical in operation. Machineries invariably used rolling elements. The performance of these rolling elements depends on stress state. The deformation which is complicated in such elements depends on the type of materials used to manufacture the elements and nature of loading. The loads are in general repetitive in nature and hence the deformation becomes much more complicated. Such complicated deformation is also called as rolling contact fatigue (RCF). The state of stress is evaluated using Hertz's stress contact theory. Such estimated stress could be used to predict deformations. The repetitive loading accompanied by Hertz's type of contact stresses leads to complication in design in such rolling elements. The literature study showed that not much of work carried out in understanding the complex deformation due to cyclic Hertz contact stresses. In the present study a four ball test rig (ASTM D 4172 standard) was used to simulate the field conditions of the bearing element. The studies were carried out both for static and dynamic conditions. High carbon high chromium steel balls are used for static study. High carbon high chromium steel, case hardened carbon steel and stainless steel balls are used for dynamic study. Lubricant SAE 20W40 was used in dynamic test. The dynamic test was carried at a 1000 rpm at varying load levels of 50N, 100N, 150N, 300N, 500N, 700N and 900N. The experiments were conducted for a period of 30 minutes. The contact radius in case of static test and co-efficient of friction in case of dynamic test was estimated. Scanning electron micrographic studies were carried on wear scar. The wear grooves which represent the non-uniform deformations were observed to be dependent on load level and type of material. At higher load level the deformation was found to be uniform with the absence of wear grooves for all materials. In general the co-efficient of friction was found to depend on the applied normal load. There was a correlation between co-efficient of friction and state of deformation.

Key Words: Rolling contact fatigue, four ball tester, Hertz contact stress

I. INTRODUCTION

The life of machine element is very important in industry from reliability and economical points of views.

Revised Manuscript Received on 30 January 2016.
* Correspondence Author
Suresha Gowda M. V, Department of Mechanical Engineering, University Visweswaraya College of Engineering, Bangalore, Karnataka, India.
Dr. Vidyasagar H. N, Department of Mechanical Engineering, University Visweswaraya College of Engineering, Bangalore, Karnataka, India.
Dr. Ranganatha S, Department of Mechanical Engineering, University Visweswaraya College of Engineering, Bangalore, Karnataka, India.

In the case of rolling elements, such as bearing, the useful life is dependent on prevailing contact stress. The prevailing contact stress which is above yield stress and in addition repetitive in nature leads to complicated deformation which is plastic and fatigue [1, 2]. The complicated deformation which leads failure of elements needs to be studied in detail. The deformations were found to be influenced by material coupled with the applied normal load, lubrication and surface finish, contact geometry and environmental conditions [3]. The complicated deformation in literature is termed as rolling contact fatigue (RCF) of hardened steel which has been widely studied [4 - 6]. The comparisons of tests for different balls were also studied [7, 8]. The literature dealing with complicated deformation and failure modes of hardened steel under conditions of contact stresses is very limited. Hence there is an important need to assess and understand the complicated deformation, performance and failure modes of bearing steels. When two bodies with non-conforming surfaces are in contact under a force, point or line contact between those bodies changes to area contact called Hertzian contact area and the stresses are developed. These stresses are called contact stresses. This concept was first experimentally and mathematically determined by Heinrich Hertz. Hertz developed a theory to calculate the contact area and pressure between the two surfaces and predicted the resulting deformation and stress induced in the objects. Hertzian contact stress forms the foundation for the equations for load bearing capabilities and fatigue life in bearings, gears, and any other bodies where two surfaces are in contact. Four ball test machine was configured according to ASTM standards. This machine is suitable for a variety of tribology test procedures. In this test rig, the upper ball is held in the collet and three lower balls held in a retainer cup without lubricating oil. The loading configuration of test assembly of four balls is shown in Fig.1.

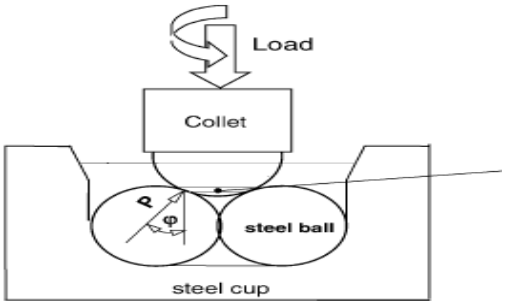

Fig. 1. Four ball tester

The procedure for calculating contact load between upper ball and lower balls, maximum contact pressure and contact radius was reported by Johnson [9].

Published By:
Blue Eyes Intelligence Engineering and Sciences Publication (BEIESP)

The relations are given below;

Contact load ***P***,

$$P = \frac{L}{3\cos\varphi} \quad (1)$$

$$p_0 = \left(\frac{6P(E^*)^2}{\pi^3(R^*)^2}\right)^{1/3} \quad (2)$$

Contact radius "*a*",

$$a = \left(\frac{3PR^*}{4E^*}\right)^{1/3} \quad (3)$$

Where

$$E^* = \left(\frac{1-\nu_1^2}{E_1} + \frac{1-\nu_2^2}{E_2}\right)^{-1} \quad (4)$$

$$R^* = \left(\frac{1}{R_1} + \frac{1}{R_2}\right)^{-1} \quad (5)$$

Where E_1 and E_2, ν_1 *and* ν_2 are the Young's modulus and Poisson's ratios of steel balls. R_1 *and* R_2 are *the* radius of the steel balls. In the present work, the complicated deformation has been studied systematically by simulating the contact stress and deformation in the laboratory. Four ball test rig which leads to Hertzian contact stress has been made use to simulate the field conditions. Experiments were conducted under static loading condition to assess the deformation under static load. Experiments were also conducted under dynamic conditions to further understand the deformation. In dynamic testing different ball materials are employed to assess the influence of material property on deformation.

II. EXPERIMENTAL DETAILS

A. Static Test

Steel balls made of high carbon high chromium steel (HCHC steel) confirming to AISI specifications are used in the static experiment. The dimension and physical properties are shown in Table.1.

Where *L* is applied load and φ is contact angle (φ= 35.3º).

Maximum contact pressure *Po*,

Table.1.Dimension and physical properties of test samples.

Property	HCHC steel
Diameter (mm)	12.7
Surface roughness *Ra* (µm)	0.024
Hardness (HRC)	60
Modulus of elasticity(GPa)	200
Poisson ratio	0.3

B. Test Procedure

The contact radius under static load was determined using four ball tester. The three lower balls were covered with white paper which was perfectly covered on the surface of the ball. The upper ball was covered with carbon paper. Static load of 1000N was loaded on to the assembly. After transfer of 1000N of load, the load was removed and ball samples were taken out from the test rig. The white paper on three lower balls was found to have a carbon impression due to load transfer from upper ball. The carbon impression was corresponding to the contact area. The radius of these areas of contact in three lower balls was measured using microscope and average was calculated. The same procedure was repeated for 2000N, 3000N, 4000N and 5000N.

C. Dynamic Test

Four ball test rig was used to conduct experiment. Where in balls of three different materials were selected. The different materials were high carbon high chromium steel, case hardened carbon steel and stainless steel. The thickness of case hardening was 0.8 mm. The chemical composition, dimension and physical properties of different materials used as balls are shown in Tables 2 and 3.

Table. 2. Chemical composition of the test balls

Material	%C	%Si	%Mn	%P	%S	%Cr
High carbon high chromium steel	**0.95-1.1**	**0.35**	**0.2-0.5**	**0.025**	**0.05**	**1.3-1.6**
Case hardened carbon steel	**0.08-0.13**	**0.10-0.35**	**0.3-0.6**	**0.04**	**0.05**	**-**
Stainless steel	**0.08**	**0.75**	**2**	**0.045**	**0.03**	**18-20**

Published By:
Blue Eyes Intelligence Engineering
and Sciences Publication (BEIESP)

Table. 3. Dimension and physical properties of test balls.

Property	High carbon high chromium steel	Case hardened carbon steel	Stainless steel
Diameter (mm)	12.7	12.7	12.7
Surface roughness *Ra* (µm)	0.024	0.024	0.024
Hardness (HRC)	60	60	39
Modulus of elasticity(GPa)	200	200	200
Poisson ratio	0.3	0.3	0.3

Experiments were conducted using four ball test rig as per ASTM (D 4172) standards. The schematic diagram of test rig is shown in **Fig.2.** The test rig was loaded with four balls, three at the bottom and one on top. All the balls are washed with acetone and dried to maintain the surfaces free from impurities. The bottom three balls were held firmly in a ball pot containing the lubricant under test and pressed against the top ball. The top ball was made to rotate at the desired speed while the bottom three balls were pressed against it.

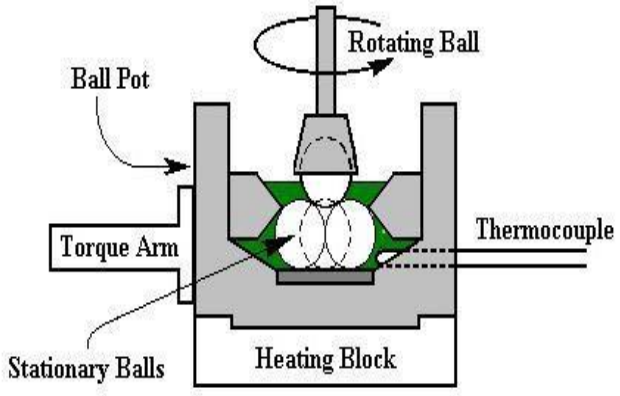

Fig. 2. Schematic Diagram of Four Ball Test Rig

D. Test Procedure

A normal load of 1kg (100N) was applied and experiment was conducted by rotating the upper ball at a speed of 1000 rpm. The experiment was conducted for running over 30 minutes. The ambient temperature was maintained at 75º C. The same procedure was repeated for loads of 3kg, 5kg, 7kg and 9kgs.In case of stainless steel experiments were conducted for loads of 50 N, 100 N and 150 N. Experiments in case of stainless steel could not be conducted at load greater than 150 N because of seizure of balls during the test. The normal load, frictional force and co-efficient of friction were monitored and recorded on a personal computer. The balls after test were carefully taken out of the test rig and the wear scar which is due to deformation of material of the balls were studied under scanning electron microscope.

III. RESULTS AND DISCUSSIONS

A. Static Test

The estimated and experimentally measured contact radius is shown in Table.4.

Table.4.Theoretically estimated contact pressure, contact radius and experimentally determined contact radius.

Sl No	Applied load (N)	Contact load (N)	Contact pressure (GPa)	Theoretical Contact radius (mm)	Experimental Contact radius (mm)
1	1000	408	4.53	0.21	0.17
2	2000	816	5.71	0.25	0.18
3	3000	1225	6.50	0.29	0.19
4	4000	1632	7.19	0.32	0.21
5	5000	2040	7.75	0.35	0.25

A plot showing the dependency of experimentally measured and theoretically estimated radius with applied load is shown in Fig.3.

Published By:
Blue Eyes Intelligence Engineering
and Sciences Publication (BEIESP)

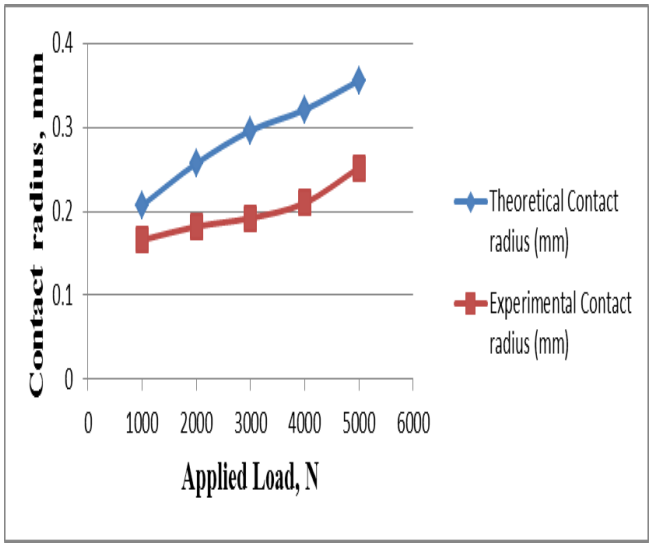

Fig. 3. Contact radius with the applied load

Experimentally determined and theoretically estimated contact radius was found to increase with normal load. The minimum value of experimentally determined contact radius was found to be 0.17mm at normal load of 1000N. The maximum value of experimentally determined contact radius was found to be 0.25mm for the 5000N normal load. The difference in theoretically estimated contact radius and experimentally obtained contact radius were found to be less at normal load of 1000N. The difference between theoretically estimated radius and experimentally determined radius was found to be more when normal load changes to 2000N, 3000N, 4000N and 5000N. The discrepancy in contact radius of theoretically estimated and experimentally determined at lower magnitude of loads being less, could be attributed to deformation of asperities on the surface. Whereas larger discrepancy in contact radius of theoretically estimated and experimentally determined at higher loads could be attributed to deformation of both asperities and bulk surface. The other possibility for the observed discrepancy in theoretically estimated contact radius and experimentally determined contact radius could be attributed to difficulty in measuring exact contact radius.

B. Dynamic Test

Few typical plots showing dependency of co-efficient of friction with time for high carbon high chromium steel, case hardened carbon steel and stainless steel are shown in Fig.4.

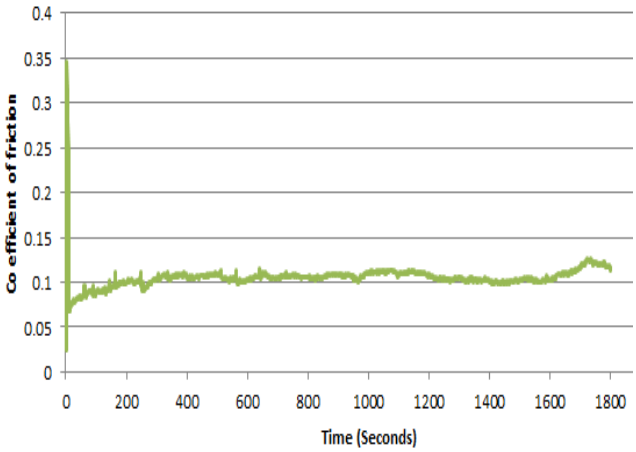

Fig. 4. (a) Dependency of co-efficient of friction with time. Material; High carbon high chromium steel. Load; 700N

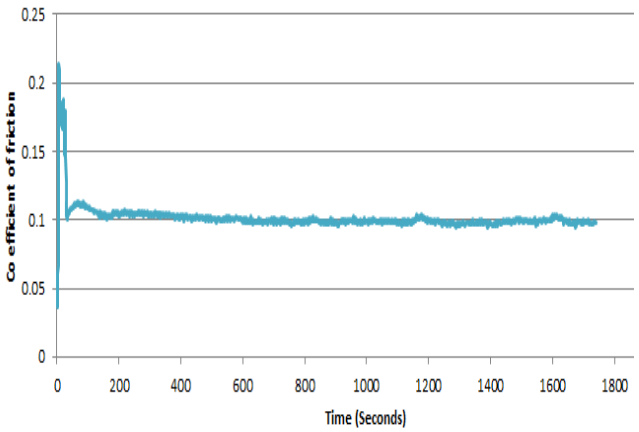

Fig. 4. (b) Dependency of co-efficient of friction with time. Material; Case hardened carbon steel. Load; 700N

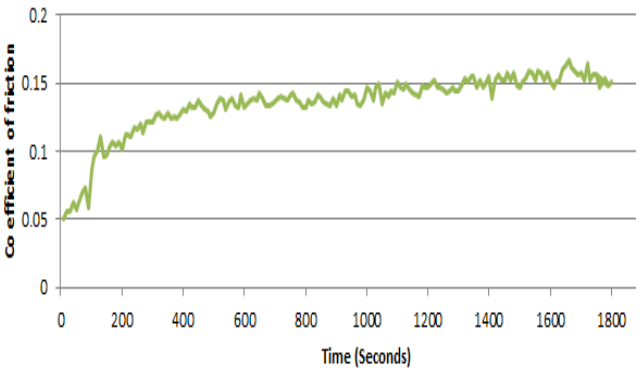

Fig. 4. (c) Dependency of co-efficient of friction with time. Material; Stainless steel. Load; 100N.

It is observed from Fig.4 that co efficient of friction for High carbon high chromium steel and Case hardened carbon steel was found to be steady after 200 seconds for load of 700N. The steady state for stainless steel was reached approximately after 400 sec. The time required to reach steady state is called running in time. As observed in static test; in discrepancy between theoretical and experimental contact radius there appears to be a relationship between running in time and extent of discrepancy between experimentally and theoretically estimated contact radius. At lower magnitude of normal load, the running in time was more and discrepancy between theoretical and experimental contact radius was less. The average co-efficient of friction in the steady state for Fig.4 was estimated for all experiments. The average co efficient of friction during steady state and the corresponding loads are shown in Table.5.

Published By:
Blue Eyes Intelligence Engineering and Sciences Publication (BEIESP)

Table.5 Applied load and co-efficient of friction for high carbon high chromium steel, case hardened carbon steel and stainless steel balls.

Applied load (N)	Co-efficient of friction (High carbon high chromium steel)	Co-efficient of friction (Case hardened carbon steel)	Co-efficient of friction (Stainless steel)
50	-	-	0.13
100	0.063	0.06	0.14
150	-	-	0.30
300	0.069	0.062	-
500	0.100	0.102	-
700	0.105	0.105	-
900	0.132	0.11	-

Average co-efficient of friction in case of high carbon high chromium steel ball is 0.063, 0.069, 0.10, 0.105 and 0.132 for loads 100N, 300N, 500N, 700N and 900N. Average co-efficient of friction in case of case hardened carbon steel ball is 0.06, 0.062, 0.102, 0.105 and 0.11 for loads 100N, 300N, 500N, 700N and 900N. The average co-efficient of friction in case of stainless steel ball is 0.13 and 0.14 for loads 50N and 100N. The average co-efficient of friction in case of stainless steel ball has been found to increase to 0.3 when load was changed to 150 N. A plot depicting the variation of co-efficient of friction with normal load for stainless steel, high carbon high chromium steel and case hardened carbon steel balls are shown in Fig.5.

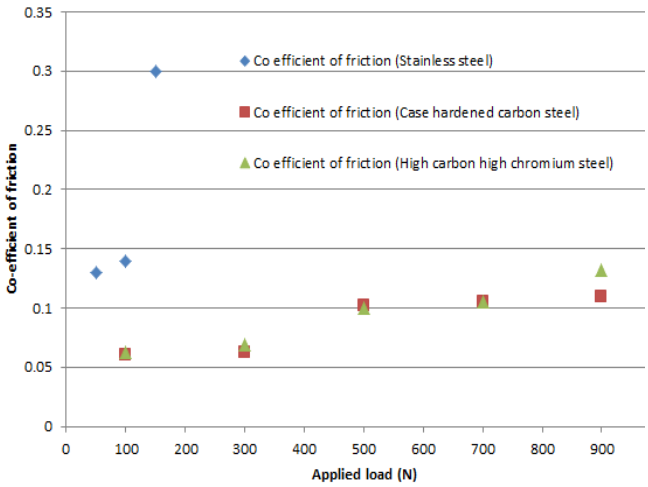

Fig. 5. Co-efficient of friction with applied load for Stainless steel, high carbon high chromium steel and case hardened carbon steel balls.

The dependency in co-efficient of fiction with normal load is shown in Fig.5.The dependency of co-efficient of fiction with normal load shown in Fig.5 indicates two distinct features. One of the feature is though the experimental normal load was more in magnitude in case of high carbon high chromium steel and case hardened carbon steel balls compared to stainless steel balls, the co-efficient of friction for stainless steel was larger. The other feature was the co-efficient of fiction for both high carbon high chromium steel and case hardened carbon steel were comparable and comparatively lower in magnitude when compared to stainless steel. In general co-efficient of fiction increased with increased load. The wear scar was studied under scanning electron microscope for identifying the possible reasons which could explain the observed variation of co-efficient of fiction of different ball materials.

C. Scanning electron micrographic studies on wear scar

The wear scar which was a result of both deformation and failure was studied in scanning electron microscope. The scanning electron micrographs of wear scar for stainless steel ball studied in scanning electron microscope for a normal load of 50N are shown in Fig.6 (a) and (b)

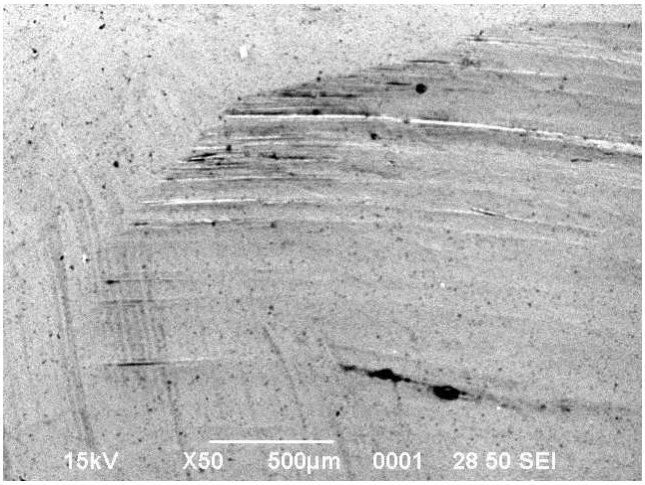

(a) Wear scar on upper ball
Load; 50N Magnification; 50X

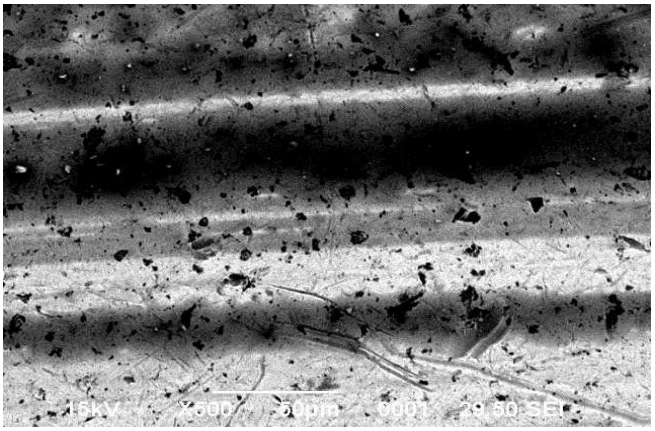

(b) Wear scar on lower ball
Load; 50N Magnification; 500X

Fig. 6. (a) and (b) Scanning electron micrographs of wear scar -stainless steel ball.

Micrograph 6(a) corresponds to load of 50N and magnification 50X. Micrograph 6(b) corresponds to load of 50N and magnification 500X. Micrograph 6(a) shows the wear deformation details at the beginning of the wear scar path. The wear grooves, results of non-uniform deformation are predominant at the top left side when compared to other areas of the scar. This variation could be attributed to variation of stress state at different area of contact.

Published By:
Blue Eyes Intelligence Engineering
and Sciences Publication (BEIESP)

The contact stresses at the outer boundaries of the wear scar are less when compared to stresses at the inner area of wear scar. At the inner area of wear scar the stresses will result in total plastic deformation. At boundaries of the contact area, the deformation was not uniform which results in formation of grooves of different intensity. Micrograph 6(b) shows the wear scar of inner contact area at higher magnification. The deformation is more uniform with regular pattern of grooves. The scanning electron micrographs of wear scar for stainless steel ball studied in scanning electron microscope for a normal load of 100N are shown in Fig.7 (a) and (b)

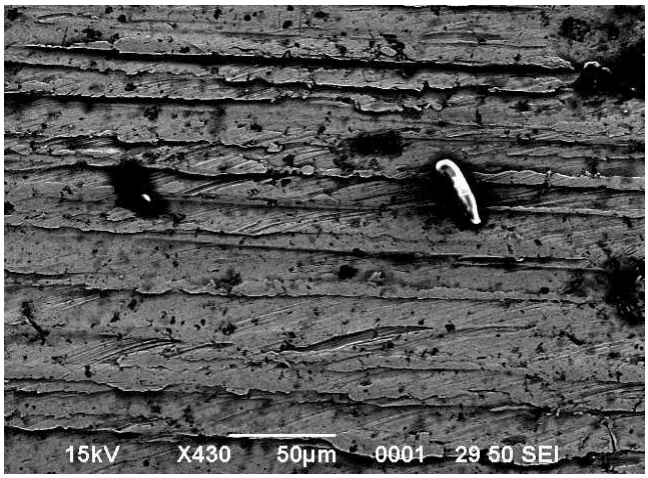

(a) Wear scar on upper ball
Load; 100N Magnification; 500X

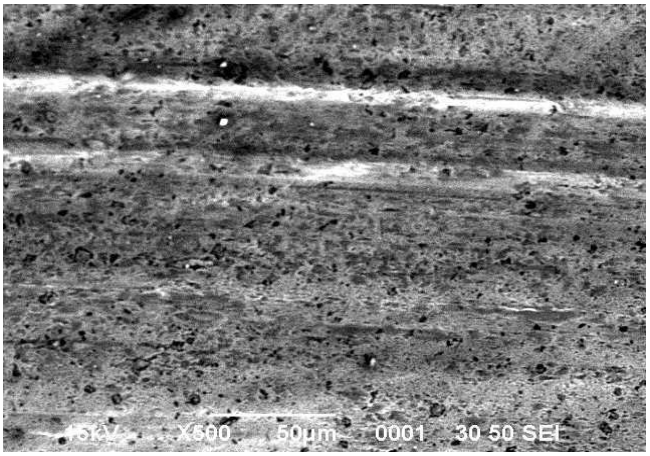

(b) Wear scar on lower ball

Load; 100N Magnification; 500X

Fig.7 (a) and (b) Scanning electron micrographs of wear scar -stainless steel ball.

The micrograph 7(a) corresponds to wear scar at end of the path whereas micrograph 7(b) corresponds to inner location of wear path. The groove patterns in micrograph 7(a) and 7(b) are different. The depth of grooves is not uniform and more number of grooves are observed in micrograph 7(a). Few and more uniform grooves are found in micrograph 7(b). The deformation is more uniform in case of micro graph 7(b) compared to micrograph 7(a). The scanning electron micrographs of wear scar for stainless steel ball studied in scanning electron microscope for a normal load of 150N are shown in Fig.8 (a) and (b)

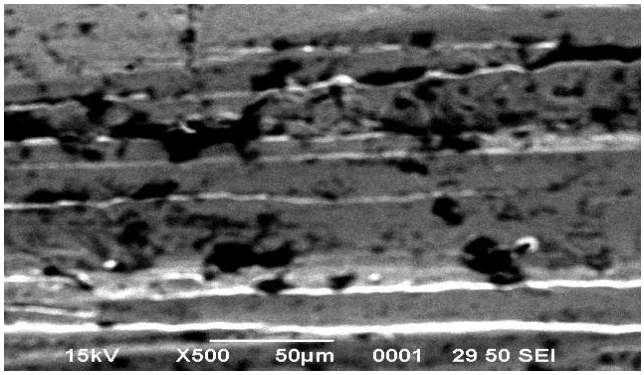

(a) Wear scar on upper ball
Load; 150N Magnification; 500X

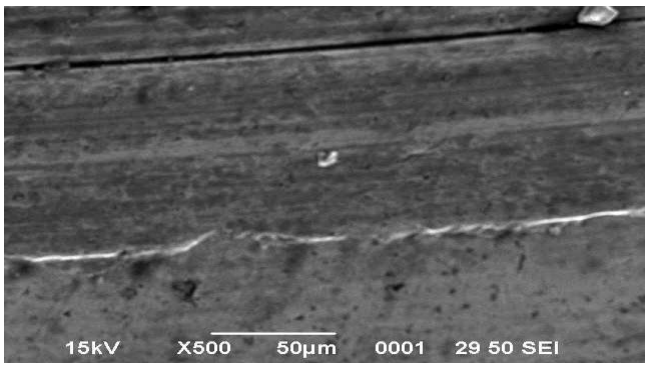

(b) Wear scar on lower ball
Load; 150N Magnification; 500X

Fig. 8. (a) and (b) Scanning electron micrographs of wear scar -stainless steel ball

The micrograph 8(a) corresponds to wear scar at end of the path whereas micrograph 8(b) corresponds to inner location of wear path. The wear groove patterns in micrograph 8(a) and 8(b) are different. More number of uneven depth wear grooves are found in micrograph 8(a). The deformation is more uniform with a few grooves in case of micrograph 8(b) compared to micrograph 8(a). The variation in number of wear grooves, their depth and spatial distribution in the wear scar as revealed in micrograph 6(b), 7(b) and 8(b) is a possible attribute of the observed increase in magnitude of co-efficient of friction with applied normal load. The scanning electron micrographs of wear scar for high carbon high chromium steel ball studied in scanning electron microscope for a normal load of 100N, 300N, 500N, 700N and 900N are shown in Fig.9 (a),(b),(c),(d) and (e)

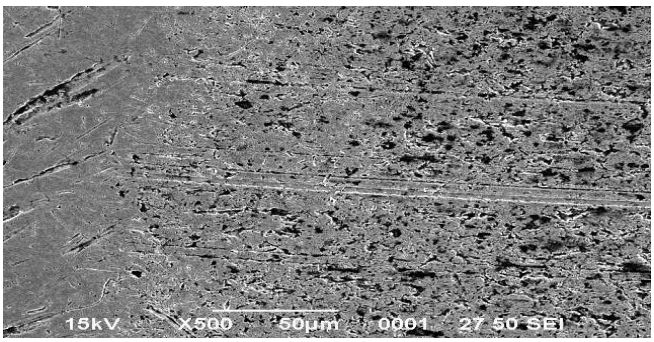

(a) Wear scar on lower ball

Load; 100N Magnification; 500X

Published By:
Blue Eyes Intelligence Engineering
and Sciences Publication (BEIESP)

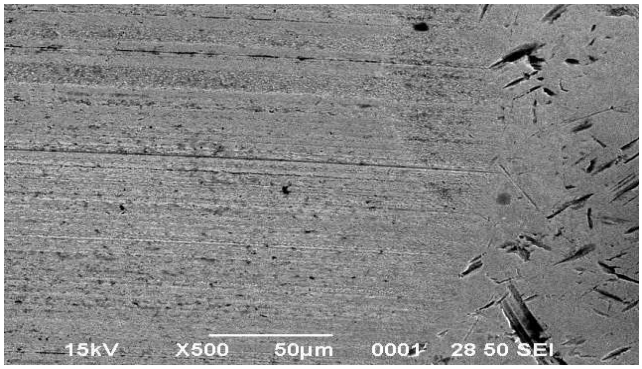

(b) Wear scar on lower ball
Load; 300N Magnification; 500X

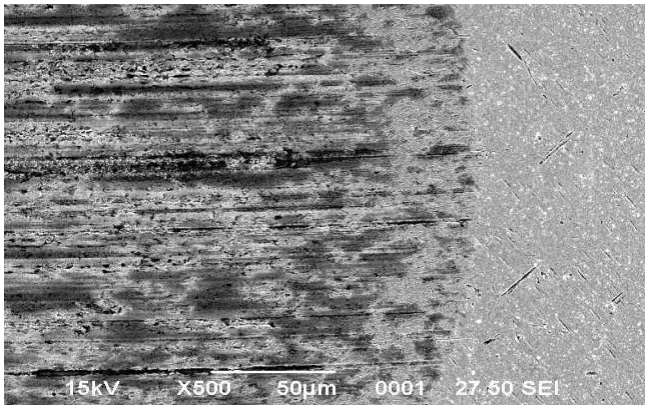

(c) Wear scar on lower ball
Load; 500N Magnification; 500X

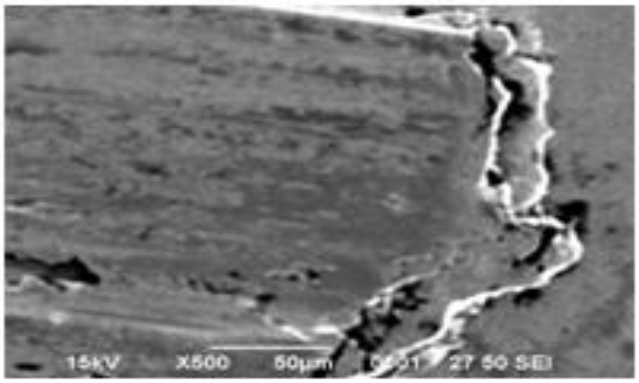

(d) Wear scar on lower ball
Load; 700N Magnification; 500X

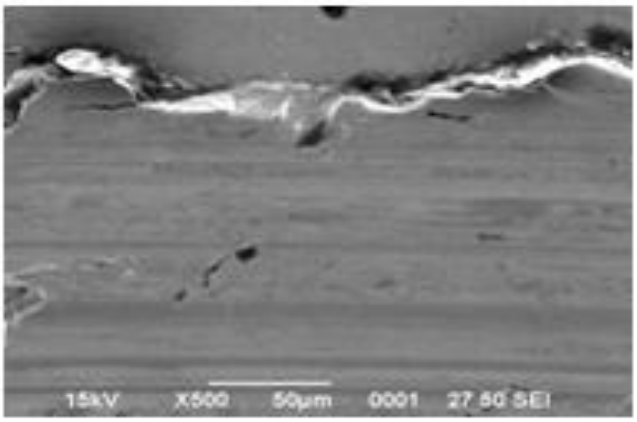

(d) Wear scar on lower ball
Load; 900N Magnification; 500X

Fig. 9. (a), (b), (c), (d) and (e) Scanning electron micrographs of wear scar -high carbon high chromium steel ball

Micrograph 9(a) corresponds to beginning of the wear path of high carbon high chromium steel ball with a normal load of 100N. The wear grooves are well defined at middle of the micrograph 9(a). The wear grooves in the other area of micrograph 9(a) are not well defined. Micrograph 9(b) corresponds to end of the wear path of high carbon high chromium steel ball with a normal load of 300N. The intensity and distribution of wear grooves in micrograph 9(b) are more compared to grooves observed in micrograph 9(a). Micrograph 9(c) corresponds to end of the wear path of high carbon high chromium steel ball with a normal load of 500N.The micrograph 9(c) shows uniform larger magnitude of plastic deformation which leads to absence of wear grooves which are consequence of non-uniform deformation. Micrograph 9(d) corresponds to end of the wear path of high carbon high chromium steel ball with a normal load of 700N.The deformation observed in micrograph 9(d) is more uniform and no grooves are observed when compared to micrographs 9(a), 9(b) and 9(c). Micrograph 9(e) shows the wear path of high carbon high chromium steel ball with a normal load of 900N. The micrograph shows no grooves and deformation is uniform. The scanning electron micrographs of wear scar for mild steel ball studied in scanning electron microscope for a normal load of 100N, 300N, 500N and 700N are shown in Fig.10 (a), (b), (c) and (d)

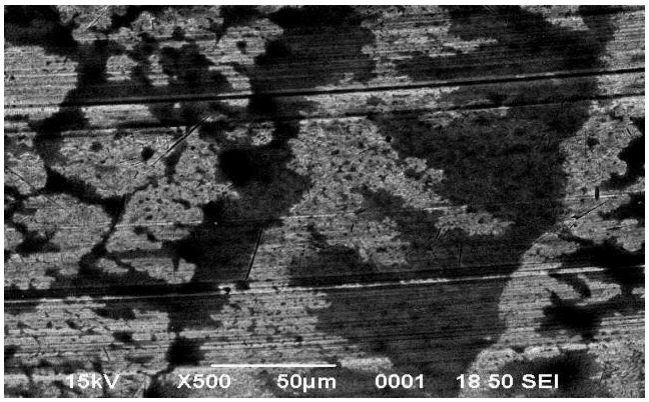

(a) Wear scar on lower ball
Load; 100N Magnification; 500X

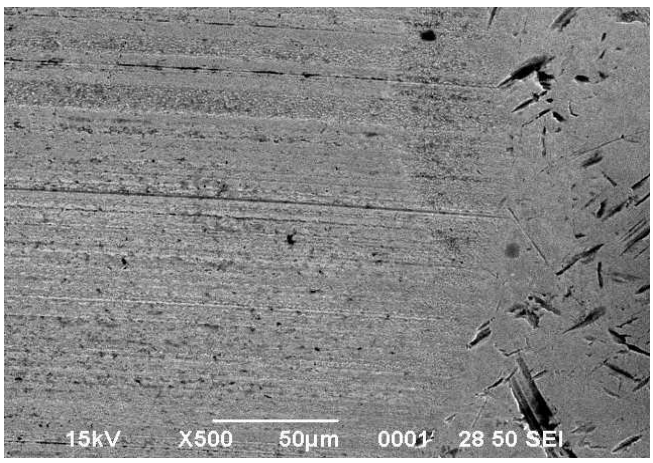

(b) Wear scar on lower ball
Load; 300N Magnification; 500X

Published By:
Blue Eyes Intelligence Engineering
and Sciences Publication (BEIESP)

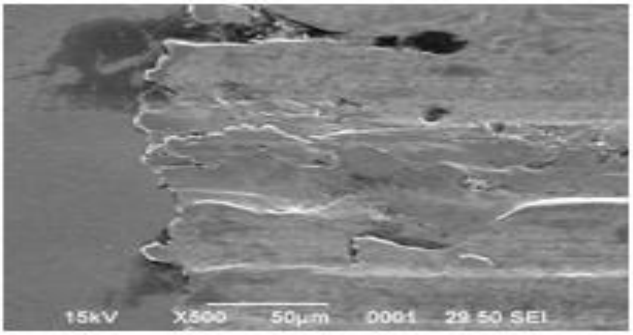

(c) Wear scar on lower ball
Load; 500N Magnification; 500X

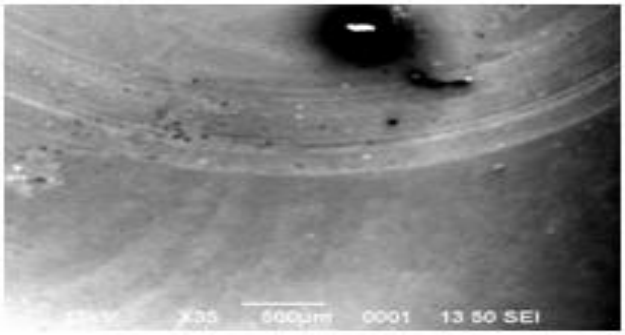

(d) Wear scar on lower ball
Load; 700N Magnification; 35X

Fig. 10. (a), (b), (c) and (d) Scanning electron micrographs of wear scar–case hardened carbon steel ball.

Micrograph 10(a) is wear path of mild steel ball for a normal load of 100N.Very few wear grooves are observed in the micrograph. Micrograph 10(b) corresponds to the end of the wear path of mild steel ball for a normal load of 300N. The wear grooves are found to be more intense and more in number compared to wear grooves found in micrograph 10(a). Micrograph 10(c) corresponds to beginning of the wear path of mild steel ball with a normal load of 500N. The deformation was found to be uniform and wear grooves are not observed. Micrograph 10(d) shows the wear path of mild steel ball with a normal load of 700N.The view of wear path for load of 700N at 500X did not reveal any special features of deformations due to intensive and uniform plastic deformation. The scanning electron micrographic study was carried out at 35X instead of 500X. The micrograph shows uniform deformation. The co-efficient of friction for stainless steel, case hardened carbon steel and high carbon high chromium steel shown in Fig.5 indicates vast difference in magnitude between stainless steel and case hardened carbon steel; high carbon high chromium steel. The comparable magnitude of co-efficient of friction for high carbon high chromium steel and case hardened carbon steel is attributed to similarity in deformation observed in Fig.9 and Fig.10. The increase in co-efficient of friction with increase in load is attributed to difference in intensity, distribution and severity of plastic deformation as observed in Fig.9 and Fig.10. Scanning electron micrographic study for different ball material was carried out to elucidate the observed difference in co-efficient of friction. Scanning electron micrographic studies of wear path of high carbon high chromium steel, case hardened carbon steel and stainless steel are carried out. The studied Scanning electron micrographs are shown in Fig.11 (a), (b) and (c).

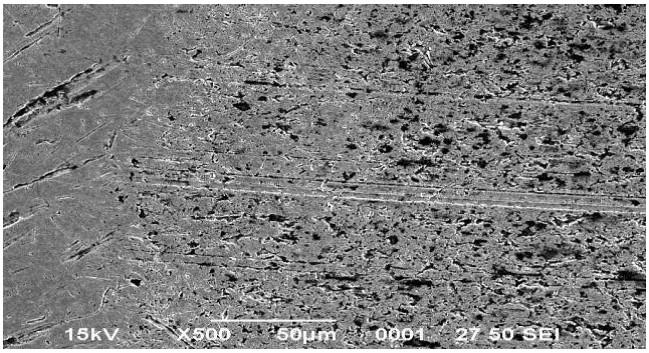

(a) Wear scar on lower ball
Load; 100N Magnification; 500X

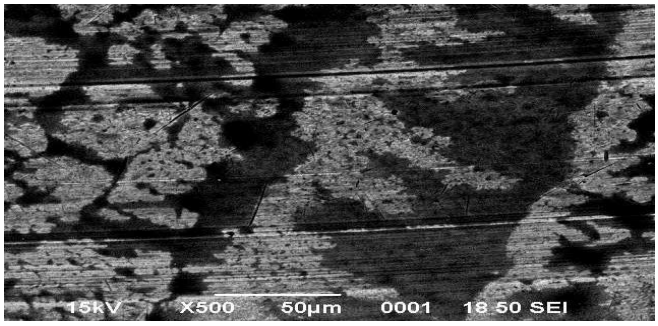

(b) Wear scar on lower ball
Load; 100N Magnification; 500X

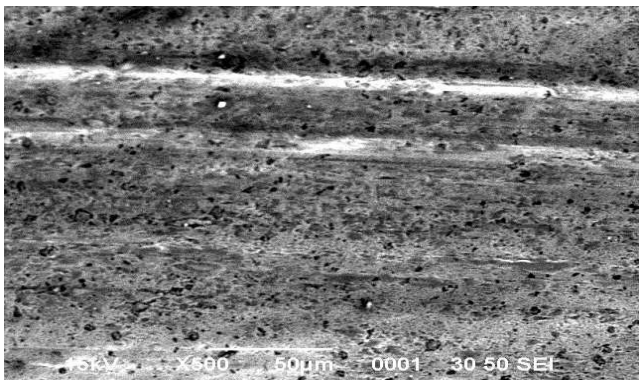

(c) Wear scar on lower ball
Load; 100N Magnification; 500X

Fig. 11. (a), (b) and (c) Scanning electron micrographs of wear scar–high carbon high chromium steel, case hardened carbon steel and stainless steel ball.

Micrograph 11(a) shows the beginning of the wear path for high carbon high chromium steel for a normal load of 100N. Micrograph 11(b) shows the beginning of the wear path for case hardened carbon steel for a normal load of 100N. Micrograph 11 (c) corresponds to wear path of stainless steel ball for a normal load of 100N.The deformation in micrograph 11(c) is observed to be more uniform when compared to deformations observed in micrograph 11(a) and 11(b). The observed larger magnitude of co-efficient of friction in case of stainless steel compared to high carbon high chromium steel and case hardened carbon steel is attributed to large scale uniform plastic deformation as observed in micrograph 11(c) compared to non-uniform and smaller amount of plastic deformation observed in micrograph 11(a) and 11(b).

Published By:
Blue Eyes Intelligence Engineering and Sciences Publication (BEIESP)

IV. CONCLUSIONS

1. Non-conforming deformations resulted in wear grooves.
2. The number of wear grooves, wear grooves depth and wear grooves distribution was found to be dependent on both load and material.
3. The wear grooves, an indication of non-uniform deformation, persisted up to the load of 500N in case of high carbon high chromium steel balls whereas wear grooves persisted up to 300N in case of case hardened carbon steel balls. After these loads the deformation observed was intense and uniform.
4. The wear grooves were observed with clarity at load of 50N in case of stainless steel balls. The wear grooves were not predominant when load was 150N.
5. The co-efficient of friction depends on the deformation state.

REFERENCES

1. R. Scott Hyde, (1996)"Contact fatigue of hardened steel", ASM Handbook, Fatigue and Fracture. Vol.19, p.1749- 1773.
2. J.E. Fernandez Rico, A. Hernandez Baltez, D. Garcia Cuervo, (2003)"Rolling contact fatigue in lubricated contacts", Tribology International, Vol. 36, p.35–40.
3. Y. wang, M. Hadfield, (2000)"The influence of ring crack location on the rolling contact fatigue failure of lubricated silicon nitride: fracture mechanics analysis", Wear, Vol. 243, p.167–174
4. B.S Kothavale,July-September(2011)"Evaluation of Extreme Pressure Properties Lubricating Oil Using Four Ball Friction Testing Machine".IJAET, Vol.2, p.56-58
5. A. Hernandez Battez, J.E. Fernandez Rico, R. Chou Rodriguez,(2005) "Rolling fatigue tests of three polyglycol lubricants" Wear, Vol. 258, p.1467–1470.
6. J. Kang, M. Hadfield, (2000) "The influence of heterogeneous porosity on silicon nitride/steel wear in bubricated rolling contact", Ceramics International, Vol. 26, p.315–324.
7. P Zhao et al., The influence of test lubricants on the rolling contact fatigue failure mechanisms of silicon nitride ceramic. Wear, Vol. 257, Issue 9-10, Nov 2004, P. 1047-1057.
8. J. Kang, M. Hadfield, December (2003) "Comparison of 4– ball and 5–ball rolling contact fatigue tests on lubricated Si3N4/steel contact", Materials and Design, Vol. 24, Issue 8, p.595– 604.
9. K. L. Johnson, (1985)"Contact mechanics", Cambridge University Press.
10. Experimental investigation of rolling contact fatigue of dented surfaces using artificial defects. Tribology and Interface Engineering Series. Vol. 48, 2005, 691-702.
11. J.Halling, Principles of tribology. 1975, Mc Millan Publications.
12. E.P.Bowden and Tabor, Friction and lubrication of solids.1954, Oxford University.

AUTHORS PROFILE

Suresha Gowda M. V, Graduated in BE (Mechanical Engineering), completed ME (Machine Design) and pursuing research in the Department of Mechanical Engineering, University Visweswaraya College of Engineering, Bangalore, Karnataka.

Dr. Vidyasagar H.N, Graduated in BE (Mechanical Engineering), completed M.Tech (Advanced Manufacturing Engineering) and PhD from UVCE Bangalore. Working as an Associate Professor in the Department of Mechanical Engineering, University Visweswaraya College of Engineering, Bangalore, Karnataka.

Dr. Ranganatha S, Graduated in BSc, BE (Mechanical Engineering), completed ME (Mechanical Engineering) and PhD from IISc Bangalore. Working as Professor in the Department of Mechanical Engineering, University Visweswaraya College of Engineering, Bangalore, Karnataka.

Published By:
Blue Eyes Intelligence Engineering
and Sciences Publication (BEIESP)